



INSTITUT DE FRANCE  
Académie des sciences

# *Comptes Rendus*

---

## *Mécanique*


Alaa Ghzayel and Anthony Beaudoin

**Three-dimensional numerical study of a local scour downstream of a submerged sluice gate using two hydro-morphodynamic models, SedFoam and FLOW-3D**

Volume 351 (2023), p. 525-550

Published online: 7 December 2023

<https://doi.org/10.5802/crmeca.223>

 This article is licensed under the  
CREATIVE COMMONS ATTRIBUTION 4.0 INTERNATIONAL LICENSE.  
<http://creativecommons.org/licenses/by/4.0/>



*Les Comptes Rendus. Mécanique sont membres du  
Centre Mersenne pour l'édition scientifique ouverte*

[www.centre-mersenne.org](http://www.centre-mersenne.org)

e-ISSN : 1873-7234



---

Spontaneous articles / *Articles spontanés*

# Three-dimensional numerical study of a local scour downstream of a submerged sluice gate using two hydro-morphodynamic models, SedFoam and FLOW-3D

*Étude numérique tridimensionnelle d'un affouillement local en aval d'une vanne submergée à l'aide de deux modèles hydro-morphodynamiques, SedFoam et FLOW-3D*

Alaa Ghzayel <sup>a</sup> and Anthony Beaudoin <sup>✉,\*,a</sup>

<sup>a</sup> Institut Pprime, SP2MI-Téléport 2, boulevard Marie et Pierre Curie, BP 30179, 86962 Futuroscope Chasseneuil Cedex, France

*E-mails:* [alaa.ghzayel@univ-poitiers.fr](mailto:alaa.ghzayel@univ-poitiers.fr) (A. Ghzayel),  
[anthony.beaudoin@univ-poitiers.fr](mailto:anthony.beaudoin@univ-poitiers.fr) (A. Beaudoin)

**Abstract.** Three-dimensional numerical simulations were performed, based on an experimental study of sediments scour process subjected to a water jet downstream of a submerged sluice gate with a rectangular opening at the bottom in a very confined channel. This experimental geometry, little studied in the literature, presents two particular phenomena in the dynamics of the scour process: a change of the dune form and a digging - refilling cycles of the scour. Two different hydro-morphodynamic models, SedFoam and FLOW-3D, were used and calibrated according to the experimental data. SedFoam is a multiphase flow model based on the open-source tool-box OpenFOAM and uses a coupling method between the fluid and particles phases in the RANS equations through the dense granular rheology, while FLOW-3D is a CFD software that uses a sediment scour model to perform sediment transport through bedload and suspended load transport equations without direct coupling with the fluid phase. The use of these specific three-dimensional numerical models in the case of the water flow with a jet in a very confined channel has allowed to evaluate the accuracy of turbulence models used. The RNG  $K-\varepsilon$  turbulence model was used in FLOW-3D while the  $K-\omega$  turbulence model was used in SedFoam. The RNG  $K-\varepsilon$  turbulence model is more numerically stable for a finer mesh size. Based on the comparison of the three-dimensional numerical results with the experimental data, a discussion has allowed to explain the two particular phenomena in the dynamics of the scour process, a change of the dune form and a digging - refilling cycles of the scour, observed in the experimental data. It was

---

\* Corresponding author.

concluded that the dune shape-shifting is due to the hydro-morphodynamic behaviour of the interaction of fluid-particles in presence of high degree of confinement while the digging - refilling phenomenon is explained by the physical mechanics behaviour of the particles phase due to gravity.

**Résumé.** Des simulations numériques tridimensionnelles ont été menées pour étudier l'affouillement des sédiments sous un jet d'eau dans un canal confiné. L'étude présente 2 phénomènes pendant l'affouillement : un changement de forme de la dune et des cycles de creusement-remplissage. Deux modèles hydro-morphodynamiques ont été utilisés et calibrés avec des données expérimentales. Les résultats ont montré que le changement de forme de dune était dû à l'interaction fluide-particules, tandis que le phénomène de creusement-remplissage était dû au comportement des particules sous l'effet de la gravité. Cette étude donne un aperçu du processus d'affouillement et de l'importance d'utiliser des modèles numériques appropriés.

**Keywords.** scouring, confined water jet, CFD modeling, turbulence modeling, multi-phase flow model, sediment scour model.

**Mots-clés.** affouillement, jet d'eau confiné, modélisation CFD tridimensionnelle, modélisation de la turbulence, écoulement multiphasique, modèle d'affouillement des sédiments.

**Funding.** The authors gratefully acknowledges the financial support of the University of Poitiers as well as the support of Flow Science, Inc. for providing a free four months FLOW-3D research licence.

*Manuscript received 2 March 2023, revised 27 June 2023, accepted 6 September 2023.*

## 1. Introduction

The water flow in the vicinity of hydraulic structures can lead to erosion of sediments around the foundations of these hydraulic structures. This occurring natural phenomenon is called scour and it is part of the natural morphological changes in river beds that can be the results of man-made hydraulic structures [1]. Scour is one of the main issues in causing failure of hydraulic structures. Predicting the geometrical shape of the local scour is necessary to predict the failure of hydraulic structures and it plays a significant role in the design of these structures [2]. The collapses of the Wilson bridge in Tours (1978) and the Saint Louis bridge in Reunion island (2007), as well as the failure of the Coarraze railway embankment on the Gave de Pau river (2013) in France, are well-known examples that raised a question on the problems caused by erosion and scouring [3]. The equipment of hydraulic structures can also cause flow conditions leading to scour of their foundations. For example, the sluice gate downstream of a hydraulic structure generates a flow jet that can cause a local scour that can affect the stability and operation of this hydraulic structure [4]. In such applications, the main condition that causes the development of the scour is the down flow impingement with the granular erodible bed [5].

The observed erosion mechanism downstream of a sluice gate of a hydraulic structure can be studied using a hydro-sedimentary channel. Many experiments in hydro-sedimentary channels were carried out for different hydraulic conditions such as the size of the opening of the sluice gate, the water tail depth, the flow rate, the lateral confinement level and the presence of an apron downstream of the sluice gate. These experiments showed the effects of these hydraulic conditions on the depth and length of the scour and the size and shape of the dune formation directly downstream of the scour hole, which can help to predict the maximum scour depth and to understand the effects of hydraulic conditions on the erosion process. During the erosion process, a scour hole and a dune just downstream of this hole are formed. The scour hole is developed rapidly at the initial stage of digging where the jet is directly impinging the granular bed. As time passes through the process of scouring, the rate of erosion decreases until it reaches an equilibrium scour hole depth [6–10].

In contrast, for certain hydraulic conditions, an equilibrium state is never reached and a phenomenon of cyclic digging and refilling of the scour is observed [7, 11]. In 2002, Lim and Yu [7], conducted 84 sets of experiments in two different channels. The first channel measures 20 m

long, 0.688 *m* deep and 0.494 *m* wide while the second is 8 *m* long, 0.3 *m* deep and 0.2 *m* wide. Lim et al. [7] discovered that for certain hydraulic conditions downstream of a solid apron located directly downstream of a sluice gate, cycles of jet flipping from the granular bed toward the free surface and vice versa were present that caused cyclic digging and refilling process with a period of 5 to 10 seconds. The refilling is due to particles rolling back until the scour is almost leveled. The apron serves as a mitigation of the scouring process through dissipating the flow energy but this erosion phenomena can still occur [7].

In 2008, Bey et al. [12] investigated the impact of channel width on scour caused by a water jet issuing from a nozzle of 2.5 *cm* under varying tailwater conditions. The study used LDA and scour profile measurements to assess the flow field and scour depth. The channel used is 16 *m* long with a variable width between 10 and 40 *cm*. It gives a ratio of channel width over nozzle height ranging between 4 and 16. Three exit velocities, 0.75, 0.9 and 1.16 *m/s*, were tested. For high submergence, Bey et al. discovered that the maximum scour depth decreases as the channel width increases from 10 to 30 *cm* for high submergence. The channel width of 40 *cm* presented a different behaviour with a higher value of the maximum scour depth. For lower submergence, Bey et al. [12] discovered that the maximum scour depth decreases as the channel width decreases. Furthermore, cycles of digging-refilling were only observed for lower submergence. The period of these cycles is influenced by the degree of confinement. Bey et al. also found that the threshold between the two submergence levels is affected by the nozzle exit velocity and that the scour and mound shape are affected by the degree of confinement [12].

In the previous studies, the smallest ratio of channel width over nozzle height tested was 4. To our knowledge, Martino et al. are the only ones to have studied values of ratio of a channel width over nozzle height lower than 4 [8]. In 2019, Martino et al. [8] studied for several values of flow rate  $Q$ , ranging from 2.5 *l/min* to 17 *l/min*, the sediment scour and the dune formation caused by a water jet downstream of a sluice gate of varying nozzle height in a very confined channel of width equal to 2 *cm* and a constant water tail depth of 13 *cm*. For values of ratio of a channel width over nozzle height lower than 2, Martino et al. [8] discovered two distinct flow dependent regimes. A steady recirculation regime was observed in lower flow rates  $Q$ . The dune changed its shape from a triangle to a trapezoidal shape at a certain time and the scour reached a maximum constant depth. For flow rates above a specific flow rate, the regime changed from a steady recirculation to digging and refilling cycles. The digging and refilling cycles were induced by a change in the direction of the flow jet. The flow jet oscillated up and down in the scour hole, significantly influencing the scouring process [8].

The comparison, between the experimental data obtained by Martino et al. [8] and the three-dimensional numerical results obtained with the hydro-morphodynamic models, can be very interesting to explain the findings made by Martino et al. [8]. In the present work, their experimental data were reproduced numerically using two different hydro-morphodynamic models, SedFoam [13] and FLOW-3D [14]. These two hydro-morphodynamic models were chosen on the basis of several aspects. SedFoam uses a complex coupled multi-phase flow RANS model for the fluid phase as well as for the particles phase while FLOW-3D uses RANS modeling for the fluid flow and a transport scouring model based on a transport equation to calculate the transport of particles. The differences between SedFoam and FLOW-3D can allow to explain the two particular phenomena observed by Martino et al.: a change of the dune shape and a digging-refilling of the scour.

SedFoam [13] is a Eulerian three-dimensional two-phase flow RANS model for the sediment transport based on the open-source toolbox, OpenFOAM. The dynamical equations are applied on both the fluid phase and the particles phase. This approach considers most physical processes where the particles phase is considered in modeling as continuum and the sediment stresses are prescribed by constitutive laws. Two important closures are implemented into the coupled RANS



equations, flow turbulence and granular stress closures. In this paper, for the flow turbulence closure, the  $K - \omega$  model is used [15]. For the granular stress closure, the dense granular flow rheology initially proposed by GDRmidi was used [16]. The full dynamics of the sediment transport through the entire computational domain is resolved without separation of the sediment transport types. SedFoam does not need the closures for bedload transport rate and the Exner equation to represent the evolution of the bathymetry of the sediment bed.

FLOW-3D is a commercial computational fluid dynamics (CFD) software which uses RANS modeling that works based on the finite volume method to solve the fluid dynamics equations as well as the volume of fluid method to track the fluid - air surface interaction. This hydro-morphodynamic model uses a three-dimensional sediment transport and scour model that is not considered as a coupled RANS multi-phase flow model. In this hydro-morphodynamic model, the fluid flow is calculated using the Reynolds averaged Navier–Stokes equations with turbulence closure but without taken the particle phase into consideration. The RNG  $K - \varepsilon$  model is used and calibrated by the software to assure numerical stability [17, 18]. As for the sediment transport, a conventional equation of the sediment transport like the Nielsen equation [19] as well as the Meyer-Peter and Muller equation [20] are implemented and used to calculate the sediment transport.

In the present work, three-dimensional numerical simulations based on both two hydro-morphodynamic models, SedFoam and FLOW-3D, are performed using the experimental setup proposed by Martino et al. in 2019 [8] as the computational domain of numerical simulations. These three-dimensional numerical simulations are performed using different flow rates  $Q$  ranging between  $6.5 \text{ l/min}$  and  $16 \text{ l/min}$  for a sluice gate aperture size  $b_0$  of  $1 \text{ cm}$ . The flow validation was made on both two models using a width of the confined channel  $w$  of  $2 \text{ cm}$  and an initial mean flow rate  $U_0$  equal to  $33.3 \text{ cm/s}$  at the sluice gate opening. The two hydro-morphodynamic models are calibrated based on the experimental data obtained by Martino et al. in 2019 [8]. The time evolution of scour depth  $Y_0$  and the maximum reached scour depth  $h$  for each flow rate  $Q$  are obtained numerically and compared with the experimental data. Moreover, the dimensionless flow velocity  $U_m/U_0$  is plotted against the experimental data in the sake of flow validation of the two hydro-morphological models. A critical time  $t_c$  when the dune undergoes shape-shifting was also deduced from the numerical results and compared with the experimental data. The main objectives of this three-dimensional numerical study are to describe the effect of lateral confinement on sediment erosion and flow jet, to describe the physical phenomena that occurred during the change of dune shape and the digging and filling cycles, and to conclude the reason behind these unique hydro-morphodynamic phenomena. This three-dimensional numerical study leads to conclusions that describe the detailed erosion behavior inside narrow lateral confined channels. The better understanding of the erosion process and the flow jet behavior in such conditions allows to facilitate the prediction of the erosion maximum depth, size and shape in hydraulic structures with high degree of lateral confinement in order to avoid complications that can lead to failure due to the intended use of these hydraulic structures due to erosion.

The structure of this paper is as follows. In Section 2, we describe the experimental setup used by Martino et al. in 2019 [8], as well as the main findings obtained from this experimental setup. In Section 3, the two hydro-morphodynamic models, SedFoam and FLOW-3D, are presented. The flow and sediment transport models used by each hydro-morphodynamic model are described. In Section 4, the mesh, the model physical parameters, the boundary conditions and the calibration are presented based on the experimental data obtained by Martino et al. [8] for the two hydro-morphodynamic models. In Section 5, the analysis of streamlines and velocity fields is performed to explain the physical mechanisms that occurred during the change of dune shape and the digging and refilling cycles. In Section 6, the analysis of the turbulence, the shear induced

pressure and the shear stress, and the sediment flux is performed to describe the effects induced by the physical mechanisms that occurred during the change of dune shape and the digging and refilling cycles. The last section is devoted to the conclusions and perspectives of this work.

## 2. Scour due to a water jet

### 2.1. Experimental setup

The three-dimensional numerical simulations, performed in this work, are based on Martino et al. hydro-sedimentary channel setup (see Fig. 1) [8]. The hydro-sedimentary channel setup is a narrow channel of dimensions 2 cm wide and 140 cm long, with glass side walls and flow rate  $Q$  controlled by a pump. In the bottom of the channel, there is a flat granular layer of 10 cm depth and 60 cm length composed of glass beads of a median diameter of 1.1 mm and density of  $2.65 \text{ g/cm}^3$ . The water depth used is 130 mm. A sluice gate is located at the upstream of the system with an aperture  $b_0$ . A rotameter measures the flow rate  $Q$  that can range from  $2.5 \text{ l/min}$  up to  $17 \text{ l/min}$ . Thus, the Reynolds number  $Re = U_0 D_h / \nu$  ranges between 3790 and 16200, where  $D_h$  is the hydraulic diameter of the opening that is represented by  $2b_0 / (1 + \frac{b_0}{w})$  and  $\nu = 0.01 \text{ cm}^2/\text{s}$  is the kinematic viscosity of water. The benchmark experiment consists of an aperture  $b_0 = 1 \text{ cm}$  that gives a  $D_h$  of 1.33 and for different values of the flow rate  $Q$  equal to 6.5, 7.5, 8.5 and  $11.5 \text{ l/min}$  that gives a  $U_0$  that ranges between  $0.54 \text{ m/s}$  and  $0.96 \text{ m/s}$ . The setup is shown in the figure below.

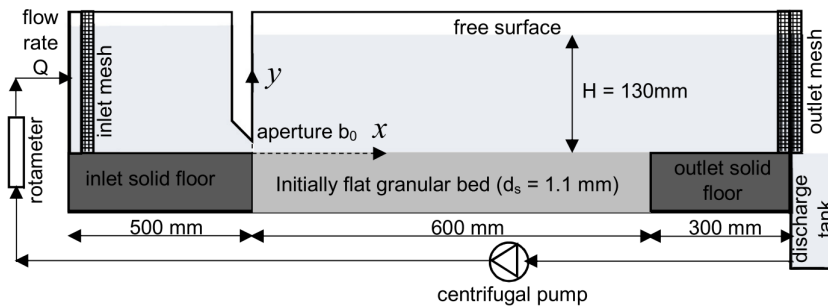


**Figure 1.** Experimental setup by Martino et al. (2019).

### 2.2. Dynamics of the scour process

To understand the physical processes, Martino et al. [8] explained that the scour formation submits two or three different phases depending on the flow rate  $Q$  (see Fig. 2 with  $Q = 6.5 \text{ l/min}$  and Fig. 3 with  $Q = 10 \text{ l/min}$ ) [8]. For a flow rate  $Q < 8.5 \text{ l/min}$ , Martino et al. [8] have observed two different phases in the time evolution of the scour hole and the form of the dune. In the first phase, the particles are extracted and transported forming a scour hole and settled downstream to the right forming a dune. This first phase is very quick (see Fig. 2  $t < 12 \text{ s}$ ). It barely took few seconds for the formation of the hole. In the second phase, the physical processes slow down and the rate of particles transport decreases. The form of the dune changes from a triangular shape to a trapezoidal shape. The more the particles accumulate, the weaker the flow jet can transport particles. It leads to accumulation of particles on the left side of the dune until the scour reaches a maximum depth and the grains on the left side of the dune migrate downslope (see Fig. 2  $t > 12 \text{ s}$ ). For a flow rate  $Q > 8.5 \text{ l/min}$ , Martino et al. have observed a third phase in the time evolution

of the scour hole and the form of the dune [8]. In this third phase, after reaching a critical value of the resistance of the dune system and when the jet is not able anymore to support this dune, the left side of the dune collapses into the scour due to gravity. Then the hole is partially refilled (see Fig. 3). These physical processes are repeated causing digging and refilling cycles.

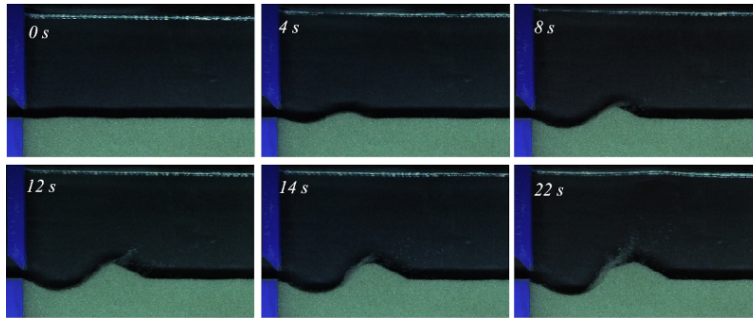


**Figure 2.** Temporal evolution of the erosion and the formation of the dune for a flow rate  $Q = 6.5 \text{ l/min}$  and  $b_0 = 1 \text{ cm}$  by Martino et al. (2019).

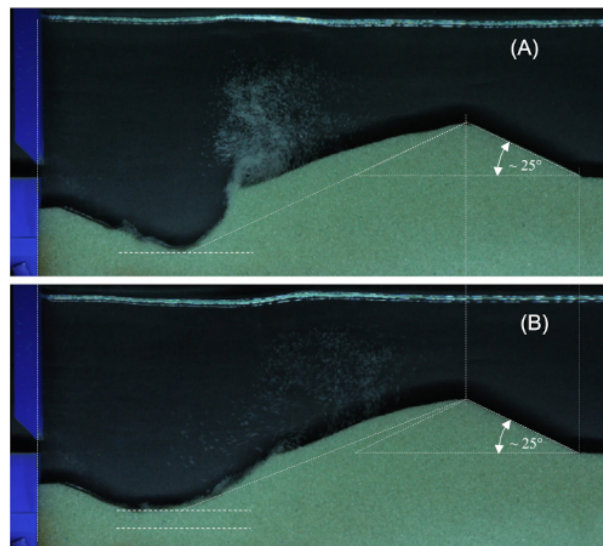


**Figure 3.** The digging-refilling phase of a flow rate  $Q = 10 \text{ l/min}$  and  $b_0 = 1 \text{ cm}$  by Martino et al. (2019).

### 3. Numerical models

#### 3.1. *SedFoam*

Two phase flow models for sediment transport have been widely developed over the past decades, in which the dynamical equations are applied to both the fluid and particles phases. In the particles phase, the particles are considered as a fluid. This approach allows us to take into account most physical processes such as particles interactions and turbulence. It is only very recently that

a 3D two-phase flow model, called SedFoam, has been applied to sediment transport by sheet flow [13, 21]. The intergranular and fluid stresses are modeled with the rheology of dense granular flow and the turbulent  $K - \omega$  model. To build the numerical model based on the Eulerian two-phase flow approach, the mass and momentum conservation equations have to be averaged over the fluid and particles phases. In order to apply this formulation to turbulent flows, turbulence averaging is also required.

The mass conservation equations are as following:

$$\frac{\partial \alpha}{\partial t} + \frac{\partial \alpha u_i^a}{\partial i} = 0, \quad (1)$$

$$\frac{\partial \beta}{\partial t} + \frac{\partial \beta u_i^b}{\partial i} = 0 \quad (2)$$

where  $\alpha$  and  $\beta$  ( $\beta = 1 - \alpha$ ) are the particles and fluid volume concentrations,  $u_i^a$  and  $u_i^b$  are the particles and fluid velocities, and  $i = x, y, z$  represents streamwise, spanwise, and vertical components, respectively. The momentum equations for the particles and fluid phases are expressed as following:

$$\frac{\partial \rho^a \alpha u_i^a}{\partial t} + \frac{\partial \rho^a \alpha u_i^a u_j^a}{\partial j} = -\alpha \frac{\partial p}{\partial i} - \frac{\partial \bar{p}^a}{\partial i} + \frac{\partial \tau_{ij}^a}{\partial j} + \alpha \rho^a g_i + \alpha \beta K (u_i^b - u_i^a) - S_{US} \beta K \nu_t^b \frac{\partial \alpha}{\partial i}, \quad (3)$$

$$\frac{\partial \rho^b \beta u_i^b}{\partial t} + \frac{\partial \rho^b \beta u_i^b u_j^b}{\partial j} = -\beta \frac{\partial p}{\partial i} + \frac{\partial \tau_{ij}^b}{\partial j} + \beta \rho^b g_i - \alpha \beta K (u_i^b - u_i^a) + S_{US} \beta K \nu_t^b \frac{\partial \alpha}{\partial i} \quad (4)$$

where  $\rho_a$  and  $\rho_b$  are the particles and fluid densities,  $p$  is the pressure of the fluid,  $\bar{p}^a$  and  $\tau_{ij}^a$  are the particles normal and shear stresses,  $\tau_{ij}^b$  is the fluid stress,  $g_i$  is the gravitational acceleration,  $S_{US}$  is the inverse of the Schmidt number  $\sigma_c$  defined as the ratio between the turbulent viscosity  $\nu_t^b$  and the turbulent diffusivity, and  $K$  is the drag parameter [21].

The drag parameter  $K$  is calculated using the following model proposed by Schiller and Naumann (1933) [22]:

$$K = 0.75 C_d \frac{\rho^b}{d_{eff}} \left\| u^b - u^a \right\| \beta^{-h_{Exp}} \quad (5)$$

where  $d_{eff} = \psi d$  is the effective sediment diameter, in which  $\psi$  is the shape factor and  $d$  is the particle diameter. The hindrance function  $\beta^{-h_{Exp}}$  represents the drag increase when the particle volume concentration increases.  $h_{Exp}$  is the hindrance exponent that depends on the particulate Reynolds number. For simplicity, the value of  $h_{Exp}$  is assumed to be equal to 2.65 for particulate Reynolds numbers lower than unity or larger than 300.  $C_d$  is a drag coefficient and it is modeled using the following expression:

$$C_d = \begin{cases} \frac{24}{Re_p} \left( 1 + 0.15 Re_p^{0.687} \right) & \text{if } Re_p \leq 1000, \\ 0.44 & \text{if } Re_p > 1000. \end{cases} \quad (6)$$

In the previous equation, the particulate Reynolds number  $Re_p$  is given by  $Re_p = \beta \|u^b - u^a\| (d_{eff}/\nu^b)$  where  $\nu^b$  is the kinematic viscosity of the fluid.

The  $K - \omega$  turbulent model is implemented into the solver. It is a two-equation model that gives a general description of turbulence by means of two transport equations that take into account the turbulent kinetic energy  $k$  and the specific turbulent energy dissipation rate  $\omega$ . The  $K - \omega$  model is more stable and suitable for near wall applications as well as for transitional flows [23]. In this model, the turbulent viscosity  $\nu_t^b$  is computed as  $\nu_t^b = k/\omega$ . The equations of the turbulent kinetic energy  $k$  and the specific turbulent energy dissipation rate  $\omega$  are a modified version of the clear fluid  $K - \omega$  equations that takes into account the particles in the fluid by adding a term for

the particle damping effect through drag and a density stratification term. The turbulent kinetic energy equation is presented as:

$$\begin{aligned} \frac{\partial k}{\partial t} + u_j^b \frac{\partial k}{\partial j} \\ = R_{ij}^{bt} \frac{\partial u_i^b}{\partial j} + \frac{\partial}{\partial j} \left[ \left( v^b + \frac{v_t^b}{\sigma_k} \right) \frac{\partial k}{\partial j} \right] - C_\mu k \omega - \frac{2K(1-t_{mf})\alpha k}{\rho^b} - \frac{S_{US}}{\beta} v_t^b \frac{\partial \alpha}{\partial j} \left( \frac{\rho^a}{\rho^b} - 1 \right) g_j \end{aligned} \quad (7)$$

and the equation of the specific turbulent energy dissipation rate  $\omega$  is written as:

$$\begin{aligned} \frac{\partial \omega}{\partial t} + u_j^b \frac{\partial \omega}{\partial j} = C_{1\omega} \frac{\omega}{k} R_{ij}^{bt} \frac{\partial u_i^b}{\partial j} + \frac{\partial}{\partial j} \left[ \left( v^b + \frac{v_t^b}{\sigma_\omega} \right) \frac{\partial \omega}{\partial j} \right] \\ - C_{2\omega} \omega^2 - C_{3\omega} \frac{2K(1-t_{mf})\alpha \omega}{\rho^b} - C_{4\omega} S_{US} \frac{\omega}{k\beta} v_t^b \frac{\partial \alpha}{\partial j} \left( \frac{\rho^a}{\rho^b} - 1 \right) g_j. \end{aligned} \quad (8)$$

In the previous equations, the values of parameters  $C_\mu$ ,  $C_{1\omega}$ ,  $C_{2\omega}$ ,  $C_{4\omega}$ ,  $\sigma_k$ , and  $\sigma_\omega$ , are equal to 0.09, 5/9, 3/40, 0.35, 0, 2, and 2.  $R_{ij}^{bt}$  is the Reynolds stress tensor defined by:

$$R_{ij}^{bt} = \rho^b \beta \left[ 2v_t^b S_{ij}^b - \frac{2}{3} k \delta_{ij} \right] \quad \text{with} \quad S_{ij}^b = \frac{1}{2} \left[ \frac{\partial u_i^b}{\partial j} + \frac{\partial u_j^b}{\partial i} \right] - \frac{1}{3} \frac{\partial u_k^b}{\partial k} \delta_{ij}. \quad (9)$$

$S_{ij}^b$  is the deviatoric part of the fluid phase strain rate tensor. An exponential function for the  $t_{mf}$  parameter was proposed by Danon et al. (1977) [24] and Chen and Wood (1985) [25], it is also utilized in the studies conducted by Kranenburg et al. (2014) [26] and Cheng et al. (2017) [27]:

$$t_{mf} = e^{-B \cdot S_t}. \quad (10)$$

In the previous equation which represents the correlation between the fluctuations of fluid and particles velocities,  $B$  is an empirical coefficient and  $S_t$  is the Stokes numbers calculated as  $S_t = t_p / t_l$  where  $t_p = \rho^a / (\beta K)$  is the particle response time and  $t_l = 1 / (0.54\omega)$  is the characteristic timescale of energetic eddie.

The particle normal stresses  $\tilde{p}^a$  can be classified into two components: a shear-induced or collisional component  $p^a$  and a permanent contact component  $p^{ff}$  [28]:

$$\tilde{p}^a = p^{ff} + p^a. \quad (11)$$

The permanent contact component  $p^{ff}$  is calculated as:

$$p^{ff} = \begin{cases} 0 & \text{if } \alpha < \alpha_{min}^{Fric}, \\ Fr \frac{(\alpha - \alpha_{min}^{Fric})^{\eta_0}}{(\alpha_{max} - \alpha)^{\eta_1}} & \text{if } \alpha > \alpha_{min}^{Fric} \end{cases} \quad (12)$$

where  $\alpha_{min}^{Fric} = 0.57$ ,  $\alpha_{max} = 0.635$  for spheres and  $Fr$ ,  $\eta_0$ , and  $\eta_1$  are empirical coefficients. The values are set to  $Fr = 0.05$ ,  $\eta_0 = 3$ , and  $\eta_1 = 5$ . The shear induced pressure  $P^a$  is defined using the following equation [21]:

$$P^a = \left( \frac{\alpha}{\alpha_{max} - \alpha} \right) \rho^a d^2 \|S^a\|^2 \quad (13)$$

where  $\|S^a\|^2$  is the norm of the shear rate tensor  $S^a$ . For modeling of the particles phase stress, the rheology of dense granular-flow is used in SedFoam. It is based on dimensional analysis. Instead of separating the collisional shear and frictional shear stresses, the total particle-phase shear stress is related to the total particle pressure  $\tilde{p}^a$  by a dynamic friction coefficient  $\mu(I)$  and the deviatoric part of strain rate tensor  $S_{ij}^a$  [29]:

$$\tilde{\tau}_{ij}^a = \mu(I) \tilde{p}^a \frac{S_{ij}^a}{\sqrt{2S_{ij}^a \cdot S_{ij}^a}} \quad \text{with} \quad S_{ij}^a = \frac{1}{2} \left[ \frac{\partial u_i^a}{\partial j} + \frac{\partial u_j^a}{\partial i} \right] - \frac{1}{3} \frac{\partial u_k^a}{\partial k} \delta_{ij}. \quad (14)$$

The friction coefficient  $\mu(I)$  depends on the inertial number  $I$ , and is computed as follows:

$$\mu(I) = \mu_s + \frac{\mu_2 - \mu_s}{I_0 I + 1} \quad \text{with} \quad I = \|\nabla u^a\| \frac{v^b}{\rho^b \bar{p}^a}. \quad (15)$$

In the previous equation,  $\mu_s$  is the static friction coefficient that ranges between 0.3 and 0.7 while  $\mu_2$  is an empirical dynamical coefficient that ranges between 0.6 and 1.2. The term  $I_0$  is an empirical constant with a value that range between 0.005 and 0.6.

### 3.2. FLOW-3D

FLOW-3D is a commercial CFD software, with a wide range of applications [14]. The software uses a special method, called TruVOE, to track the free surface. This method is an improved form beyond the original volume of fluid technique which increases the accuracy of tracking interfaces at the boundary conditions [30]. The FAVOR (fractional area-volume obstacle representation) method is also used to locate and simulate surfaces and rigid geometric regions [31]. The continuity and momentum equations based on the Reynolds Averaged Navier–Stokes (RANS) equations are the governing equations used to compute the fluid motions. To solve the RANS equations, the software uses the finite volume method.

The general form of the continuity equation is as following:

$$V_F \frac{\partial \rho_f}{\partial t} + \frac{\partial}{\partial x} (\rho_f u A_x) + \frac{\partial}{\partial y} (\rho_f v A_y) + \frac{\partial}{\partial z} (\rho_f w A_z) = R_{DIF} + R_{SOR}. \quad (16)$$

In the previous equation, on the left-hand side,  $V_F$  is the fractional volume open to flow and  $\rho_f$  is the fluid density. The components,  $u$ ,  $v$  and  $w$ , are the velocity components in the coordinate directions  $x$ ,  $y$  and  $z$ , respectively. The parameters  $A_x$ ,  $A_y$  and  $A_z$  are the fractional volume open to flow in the coordinate directions  $x$ ,  $y$  and  $z$ , respectively. On the right-hand side of the previous equation, the parameter  $R_{DIF}$  is a turbulent diffusion term while the parameter  $R_{SOR}$  represents the mass source. The fluid velocity components,  $u$ ,  $v$  and  $w$ , are expressed using the RANS equations as follows [32]:

$$\frac{\partial u}{\partial t} + \frac{1}{V_F} \left( u A_x \frac{\partial u}{\partial x} + v A_y \frac{\partial u}{\partial y} + w A_z \frac{\partial u}{\partial z} \right) = -\frac{1}{\rho_f} \frac{\partial P}{\partial x} + G_x + f_x, \quad (17)$$

$$\frac{\partial v}{\partial t} + \frac{1}{V_F} \left( u A_x \frac{\partial v}{\partial x} + v A_y \frac{\partial v}{\partial y} + w A_z \frac{\partial v}{\partial z} \right) = -\frac{1}{\rho_f} \frac{\partial P}{\partial y} + G_y + f_y, \quad (18)$$

$$\frac{\partial w}{\partial t} + \frac{1}{V_F} \left( u A_x \frac{\partial w}{\partial x} + v A_y \frac{\partial w}{\partial y} + w A_z \frac{\partial w}{\partial z} \right) = -\frac{1}{\rho_f} \frac{\partial P}{\partial z} + G_z + f_z. \quad (19)$$

In the previous equations, the parameter  $P$  is the pressure, the terms  $G_x$ ,  $G_y$  and  $G_z$  represent the accelerations of gravity in the coordinate directions,  $x$ ,  $y$  and  $z$ , while the terms  $f_x$ ,  $f_y$  and  $f_z$  represent the viscous forces in the coordinate directions  $x$ ,  $y$  and  $z$ .

To solve the RANS equations, a turbulence closure is required. FLOW-3D includes several turbulence models, such as the  $K - \omega$ ,  $K - \epsilon$  and RNG  $K - \epsilon$  turbulent models. In this work, the RNG  $K - \epsilon$  was used since it provided numerical stability over the other models in our case study. The RNG  $K - \epsilon$  model is a modified version of the  $K - \epsilon$  model. It uses equations similar to the equations for the  $K - \epsilon$  model. However, the equation constants that are found empirically in the standard  $K - \epsilon$  model are derived explicitly in the RNG  $K - \epsilon$  model. Moreover, the RNG  $K - \epsilon$  model is known to describe low intensity turbulence flows and flows having strong shear regions, as well as flows that submit recirculation and swirling flows [33]. The RNG  $K - \epsilon$  model consists

of two equations, the turbulent kinetic energy  $k_T$  and the kinetic energy dissipation  $\varepsilon_T$  equations as following:

$$\frac{\partial k_T}{\partial t} + \frac{1}{V_F} \left( u A_x \frac{\partial k_T}{\partial x} + v A_y \frac{\partial k_T}{\partial y} + w A_z \frac{\partial k_T}{\partial z} \right) = P_T + G_T + Diff_T - \varepsilon_T, \quad (20)$$

$$\frac{\partial \varepsilon_T}{\partial t} + \frac{1}{V_F} \left( u A_x \frac{\partial \varepsilon_T}{\partial x} + v A_y \frac{\partial \varepsilon_T}{\partial y} + w A_z \frac{\partial \varepsilon_T}{\partial z} \right) = \frac{CDIS1}{k_T} (P_T + CDIS3.G) + Diff_\varepsilon - CDIS2 \frac{\varepsilon_T^2}{k_T}. \quad (21)$$

In the equation of the turbulent kinetic energy  $k_T$ ,  $P_T$  is the turbulent kinetic energy production,  $G_T$  is the buoyancy production term and  $Diff_T$  is a turbulent diffusion term. In the equation of dissipation of turbulent kinetic energy  $\varepsilon_T$ ,  $CDIS1$ ,  $CDIS2$  and  $CDIS3$  are dimensionless parameters. The values of these parameters are the difference between the standard  $K - \varepsilon$  model and the RNG  $K - \varepsilon$  model. For the RNG  $K - \varepsilon$  model,  $CDIS1$  and  $CDIS3$  take the values of 1.42 and 0.2 respectively while  $CDIS2$  is computed from the turbulent kinetic energy  $k_T$  and the turbulent production term  $P_T$ . The kinetic turbulent viscosity  $\nu_T$  is calculated from the following expression:

$$\nu_T = CNU \frac{k_T^2}{\varepsilon_T}. \quad (22)$$

The term  $CNU$ , in the turbulent kinetic viscosity expression, takes the value of 0.085.

A sediment scour model is used in FLOW-3D. In this model, multiple non-cohesive sediments species with different properties can be included. The value of properties is user-specified. The values of the grain size, the mass density, the critical shear stress, the angle of repose and the sediment entrainment can be defined manually in the model. In this model, the sediments can exist in two different states, suspended sediments as well as packed sediments. The packed sediments are presented using a user-defined critical packing fraction. The surface layer of the sediment grain bed can move in the form of a bed-load using a transport equation. To predict the critical shield parameter, the Soulsby–Whitehouse equation is used [34]. This parameter can also be defined by the user, with a default value of 0.05.

To calculate the critical shield parameter, the first step is to calculate the dimensionless parameter  $d_{*,s}$  using the following expression:

$$d_{*,s} = d_s \left[ \frac{\rho_f (\rho_s - \rho_f) \|g\|}{\nu_f^2} \right]^{1/3}. \quad (23)$$

In the previous expression,  $\rho_s$  is the sediment species density,  $d_s$  is the grain diameter,  $\nu_f$  is the fluid kinematic viscosity and  $\|g\|$  is the magnitude of the acceleration of gravity. Using the previous parameter  $d_{*,s}$ , the dimensionless critical Shields number  $\theta_{cr,s}$  is calculated using the Soulsby–Whitehouse equation expressed as:

$$\theta_{cr,s} = \frac{0.3}{1 + 1.2d_{*,s}} + 0.055 [1 - \exp(-0.02d_{*,s})]. \quad (24)$$

The local number of Shields  $\theta_s$  is calculated using the local bed shear stress  $\tau$  with the following expression:

$$\theta_s = \frac{\tau}{\|g\| d_s (\rho_s - \rho_f)}. \quad (25)$$

The bed-load transport is the form of the sediment transport where the grains move through sliding, bouncing and rolling along the bed. In the model, the bed-load transport rate is computed using one of three bed-load transport equations, Meyer–Peter and Müller [20], Van Rijn [35] and

Nielsen [19] equations. In the performed numerical simulations, the Nielsen equation was used by taking the following dimensionless bed-load transport rate  $\phi_s$  expression:

$$\phi_s = \beta_{Nie,s} \theta_s^{0.5} (\theta_s - \theta_{cr,s}). \quad (26)$$

In the previous equation,  $\beta_{Nie,s}$  is a coefficient of transport that is typically equal to 12, but it can be modified by the user. Using  $\phi_s$ , the volumetric bed-load transport rate  $q_{b,s}$  can be computed using the expression:

$$q_{b,s} = \phi_s \left[ \|g\| \left( \frac{\rho_s - \rho_f}{\rho_f} \right) d_s^3 \right]^{1/2}. \quad (27)$$

Moreover, the concentration of the suspended load  $c$  is calculated using the advection and diffusion equation presented in the FAVOR method as following:

$$\frac{\partial c}{\partial t} + \frac{1}{V_F} \left( \frac{\partial A_x u c}{\partial x} + \frac{\partial A_y v c}{\partial y} + \frac{\partial A_z w c}{\partial z} - \frac{\partial A_z w_f c}{\partial z} \right) = \frac{D_t}{V_F} \left( \frac{\partial}{\partial x} \left( A_x \frac{\partial c}{\partial x} \right) + \frac{\partial}{\partial y} \left( A_y \frac{\partial c}{\partial y} \right) + \frac{\partial}{\partial z} \left( A_z \frac{\partial c}{\partial z} \right) \right) \quad (28)$$

where  $w_f$  is the dropping velocity of the sediment and  $D_t$  is the eddy diffusion coefficient equal to  $1.25\nu_t$ . Finally, the morphological change in the sediment bed is estimated by the following sediment mass continuity equation:

$$\frac{\partial Z}{\partial t} + \frac{1}{S(1-\lambda)} \left( \frac{\partial L_x q_{b,x}}{\partial x} + \frac{\partial L_y q_{b,y}}{\partial y} + S(q_{su} - w_f c_b) \right) = 0 \quad (29)$$

where  $Z$  is the bed elevation,  $\lambda$  is the bed porosity,  $S$  is the fractional area on 2DH bed-plane,  $L_x$  and  $L_y$  represent the fractional on 2DH bed-plane.  $q_{su}$  is the suspended-load transport rate per unit area calculated by the Itakura and Kishi's formula.  $c_b$  is the near bed suspended concentration.

## 4. Calibration and validation

### 4.1. Three-dimensional mesh creation

A calibration of the mesh cell size was first necessary to achieve numerical results close to the experimental data. The mesh is build using Snappyhexmesh and the blockMesh utility of OpenFoam for SedFoam while a built-in mesh tool in FLOW-3D was used. A uniform three-dimensional square mesh was used (see Fig. 4). For the mesh cell size in the  $x$ ,  $y$  and  $z$  directions, an initial cell size  $\Delta_x = \Delta_y = \Delta_z$  that is close to the mean grain size  $d_m$  which is  $1.1 \text{ mm}$  was proposed taking into consideration the numerical stability of the numerical simulations for the smaller cell size and avoiding the low accuracy of numerical results for the larger cell size. Moreover, walls boundary conditions were considered on the sides of the computational domain. The proposed starting cell size was  $1.25 \text{ mm}$ . The tests were done on SedFoam, using the  $K - \omega$  turbulence model [23] and on FLOW-3D, using the RNG  $K - \epsilon$  turbulence model [33]. Only, FLOW-3D using the RNG  $K - \epsilon$  turbulence model has allowed to simulate correctly the flows. For SedFoam, since the RNG  $K - \epsilon$  turbulence model is not implemented, it couldn't be tested. A bigger cell size of  $2.5 \text{ mm}$  was the minimum size that can achieve numerical stability without losing the accuracy of numerical results. This calibration of the mesh cell size highlighted the importance of the numerical stability that the RNG  $K - \epsilon$  turbulence model can achieve in the configuration of a turbulent multi-phase flow subjected to flow re-circulation.



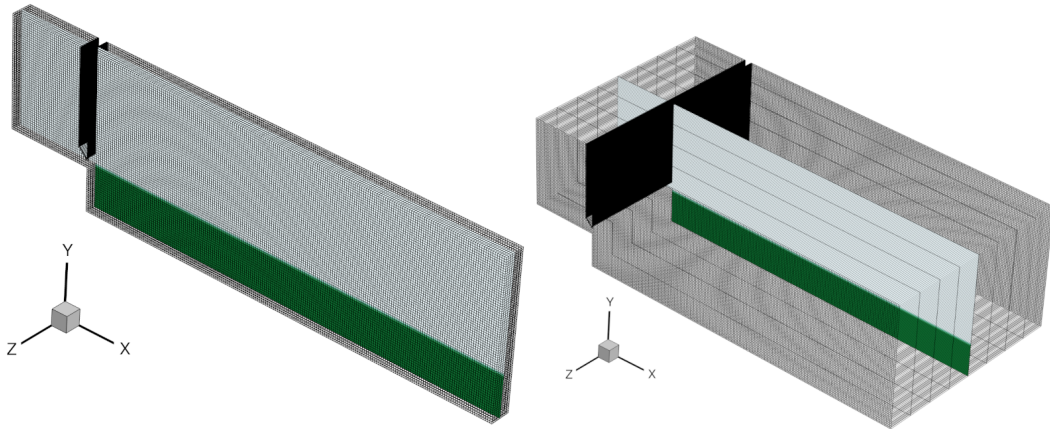


**Figure 4.** 3D uniform mesh of the computational domain with a mid cut to represent results in the middle of the domain. Original mesh (a) and scaled width ( $\times 30$ ) for better observation (b).

#### 4.2. Model physical parameters

To calibrate the hydro-morphodynamic models to the experimental data, some user defined parameters had to be chosen carefully to achieve the appropriate numerical results. For both hydro-morphodynamic models, the characteristics of water are identical: fluid density  $\rho^b$  (or  $\rho_f$ ) =  $1000 \text{ kg/m}^3$  and kinematic viscosity of the fluid  $\nu^b$  (or  $\nu_f$ ) =  $10^{-6} \text{ kg/m/s}$ . And the gravity is vertical and equal to  $9.81 \text{ m/s}^{-2}$ .

In SedFoam, the particle density  $\rho_a$  is defined as  $2650 \text{ kg/m}^3$ . For the effective sediment diameter  $d_{eff}$  used to estimate the particulate Reynolds number  $Re_p$ , the particles diameter  $d$  and the shape factor  $\psi$  are defined as  $1.1 \text{ mm}$  and  $1$ , respectively. For the parameter  $t_{mf}$ , the empirical coefficient  $B$  is equal to  $0.25$ . For the friction coefficient  $\mu(I)$ , the static friction coefficient  $\mu_s$  was defined as the tangent of the repose angle of used materials, chosen as  $\theta = 25^\circ$ . For the two other parameters,  $\mu_2$  and  $I_0$ , a sensitivity test has given  $0.7$  and  $0.6$ , respectively.

In FLOW-3D, several parameters had been defined, the repose angle is taken as  $\theta = 25^\circ$ , the maximum packing volume fraction  $\alpha$  is given the value of  $0.59$  while the diameter  $d_s$  of grains and the density  $\rho_s$  and the bed porosity  $\lambda$  are defined as  $1.1 \text{ mm}$ ,  $2650 \text{ kg/m}^3$ , and  $0.4$  respectively. For the sediment transport model, the Nielson equation is chosen with a bed load coefficient  $\beta_{Nie,s}$  equal to  $12$  (see Eq. (26)) and a bed roughness  $k_s/d_s$  of a value of  $7$  and an entrainment coefficient  $E_c$  equal to  $2$ . This bed load equation with these user defined parameters was chosen because it gave the adequate maximum scour depth. The critical Shields number  $\theta_{cr,s}$  was calculated numerically using the Soulsby-Whitehouse equation option implemented into the model (see Eq. (24)).

All the three-dimensional numerical simulations have been performed on a computing machine equipped with two Intel(R) Xeon(R) CPU E5-2683 v4 @ 2.10GHz and 256 Gb of RAM. Each CPU is composed of 16 processors. To simulate 30 seconds in real time requires a CPU time of 7 days using SedFoam and 5 days using FLOW-3D.

#### 4.3. Boundary conditions

To initiate numerical simulations in the hydro-morphodynamic model FLOW-3D, boundary conditions have to be specified. For the inlet of the computational domain, the boundary condition,

called *volume flow rate*, is used. It allows to fix a constant flow rate in  $m^3/s$ . For the outlet of the computational domain, the boundary condition, called *outflow*, is used to drive the flow outside of the computational domain. For both the left and right sides, as well as the bottom side, the boundary condition, called *wall*, is set to simulate the effect of a wall. These boundary conditions are similar to those used by Ghasemi and Soltano [36]. For the top side of the computational domain, a free surface is used as a boundary condition. Initially, a water height is specified inside the computational domain and a air layer is initialized on the top of the water layer. Here, the VOF method is used to track the free surface of water.

In the hydro-morphodynamic model SedFOAM, the boundary conditions are used according to the works by Chauchat et al. [13]. For the inlet of the computational domain, a constant velocity is fixed by using the boundary condition called *fixedValue*. For the outlet of the computational domain, the boundary condition, called *zeroGradient*, is specified. For the other boundaries of the computational domain, left, right and bottom sides, the boundary condition called *wall* is used. In contrast to FLOW-3D, SedFOAM does not allow to simulate the free surface of water. SedFOAM imposes the boundary condition called *zeroGradient* on the top of the computational domain. In SedFOAM, a free surface tracking is not available.

#### 4.4. Confined Flow

To assure that the two hydro-morphodynamic models, SedFoam and FLOW-3D, simulate correctly the water flow, the numerical results are compared to the experimental data through the dimensionless maximum velocity  $U_m/U_0$  where  $U_m$  is the maximum velocity of the jet and  $U_0$  is the initial mean velocity at the sluice gate calculated as  $U_0 = Q/(wb_0)$ . A sluice gate with an aperture  $b_0 = 2 \text{ cm}$  was used. The erodible particles bed was replaced with a smooth non-erodible bed. A flow rate  $Q = 8 \text{ l/min}$  that gives an initial mean velocity  $U_0$  equal to  $33.3 \text{ cm/s}$  is considered. Experimentally, the vertical profile of the flow velocity was measured at several stations located at a distance  $x$  from the sluice gate. A velocity decay was observed at increasing distance from the sluice gate, with the dimensionless maximum velocity  $U_m/U_0$ . It can be described by the expression following:

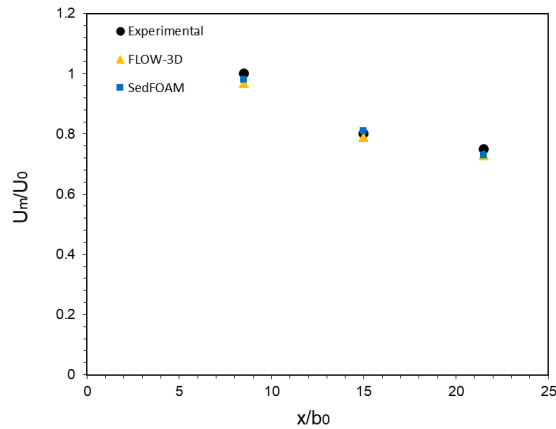
$$\frac{U_m}{U_0} = 2 \left( \frac{x}{b_0} \right)^{-1/3} . \quad (30)$$

Fig. 5 presents the values of the ratio  $U_m/U_0$  obtained with the experimental setup proposed by Martino et al. [8] and the two hydro-morphodynamic models, SedFoam and FLOW-3D, at several stations located at a distance  $x$  from the sluice gate. SedFoam and FLOW-3D give numerical results close to the experimental data. The velocity decay along the channel is correctly simulated by both models.

#### 4.5. Temporal evolution of the scour depth

To assure that the two hydro-morphodynamic models, SedFoam and FLOW-3D, simulate correctly the sediment transport, the numerical results are compared to the experimental data through the time evolution of the maximum scour depth  $Y_0$ , the critical time  $t_c$  and the maximum scour depth  $h$ . The critical time  $t_c$  corresponds to the time when the dune submits a change from a triangular shape to a trapezoidal shape. The numerical simulations, performed with SedFoam and FLOW-3D, correspond to experimental data obtained for four different values of the flow rate  $Q = 6.5, 7.5, 8.5$  and  $11.5 \text{ l/min}$  with an aperture  $b_0$  equal to  $1 \text{ cm}$  and a water depth of  $13 \text{ cm}$  in a channel of width  $w$  equal to  $2 \text{ cm}$ .

In Fig. 6, the time evolution of the maximum scour depth  $Y_0$ , measured with the experimental data and simulated with the two hydro-morphodynamic models, is presented for each flow



**Figure 5.** Variation of the dimensionless maximum Velocity  $U_m/U_o$  in function of  $x/b_0$  for a flow rate  $Q = 8 \text{ l/min}$ .

rate  $Q$  considered. It should be noted that the numerical simulations were only performed for a short period of time because the numerical simulations are very time consuming while the experimental data went all the way to several hours. Only the first period of numerical results and experimental data were compared. No long scouring period simulations were performed due to the enormous CPU time.

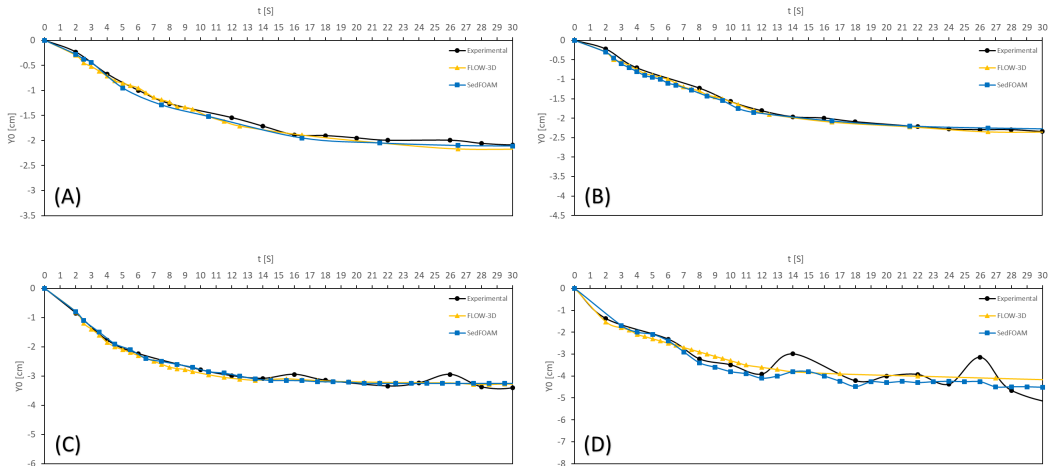


**Figure 6.** Time evolution of the maximum scour depth  $Y_0$  for several flow rates  $Q$  of  $6.5 \text{ l/min}$  (A),  $7.5 \text{ l/min}$  (B),  $8.5 \text{ l/min}$  (C) and  $11.5 \text{ l/min}$  (D).

For all the tested values of the flow rate  $Q$ , the numerical results show a general good agreement with the experimental data. SedFoam and FLOW-3D have the same erosion behavior as the experimental data where the rate of the erosion is higher at the first few seconds and then it reaches a steady low rate of erosion before reaching a steady scour depth. Moreover, for lower flow rates, it is noted that both hydro-morphodynamic models reach almost the same depth as the experimental data which concludes that both hydro-morphodynamic models are able to

predict the maximum scour depth that is essential for hydraulic structure failure prevention. For the flow rate  $Q = 11.5 \text{ l/min}$ , where the experimental data presented an oscillation in the maximum scour depth (see Fig. 6-D), FLOW-3D and SedFoam predicted an average value for the maximum scour depth. This predicted depth is between the oscillation of the experimental data but still close enough to predict max scour depth with an error lower than 6 %. Fig. 7 presents the critical time  $t_c$  (left) and the maximum scour depth  $h$  (right) as functions of the flow rate  $Q$ . For  $t_c$ , the numerical results are in good agreement with the experimental data except with the flow rate  $Q = 11.5 \text{ l/min}$  where there was a small difference of 1 to 2 seconds which is relatively low. For  $h$ , the numerical results show that SedFoam and FLOW-3D allow to simulate correctly the maximum scour depth.

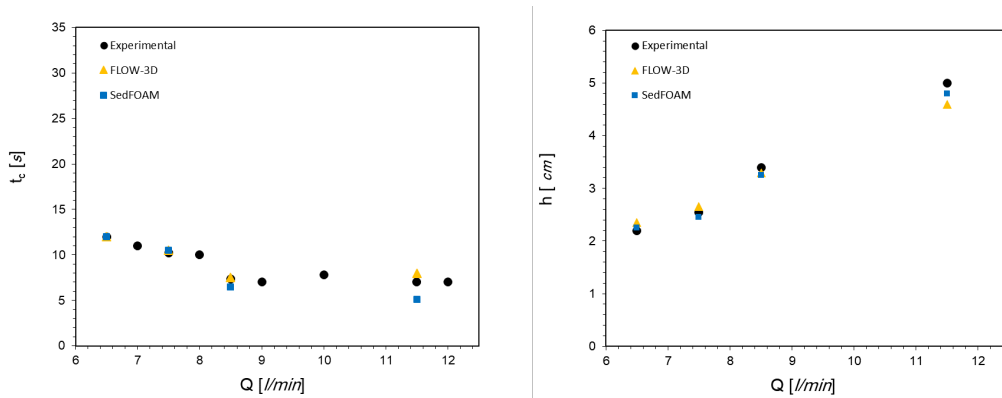


**Figure 7.** Critical time  $t_c$  (left) and maximum scour depth  $h$  (right) as functions of the flow rate  $Q$ .

In the previous numerical simulations, no digging and refilling cycles are observed on both hydro-morphodynamic models for flow rates equal and lower than  $8.5 \text{ l/min}$ , while in the experimental data cycles of digging and refilling were observed for flow rates  $Q$  higher or equal to  $8.5 \text{ l/min}$ . For flow rates  $Q$  ranging between  $6.5 \text{ l/min}$  and  $8.5 \text{ l/min}$ , the numerical simulations behaved as a steady re-circulation regime. It means that no refilling occurred in the scour hole and the maximum depth of the scour hole  $h$  is reached and stabilized. In contrast, for a flow rate  $Q = 11.5 \text{ l/min}$ , in the numerical results using SedFoam, small oscillations are observed. To validate these numerical results obtained with SedFoam, the flow rate  $Q = 16.5 \text{ l/min}$  is then tested numerically with an aperture  $b_0$  equal to  $1 \text{ cm}$  to check if the behavior will always stay as a steady re-circulation regime or will behave differently in the numerical simulations for higher flow rates. The experimental data for the flow rate  $Q = 16.5 \text{ l/min}$  with the same sluice gate aperture is not available. The numerical simulation is an attempt to reproduce cycles of digging and refilling to explain numerically this phenomenon. In Fig. 8, the time evolution of the maximum scour depth  $Y_0$  obtained with the hydro-morphodynamic model SedFoam with all the flow rates is presented. We can observe that the value of the maximum scour depth  $Y_m$  oscillates starting from a flow rate  $Q = 11.5 \text{ l/min}$ . It indicates that a refilling phase follows a digging phase and this regime repeats in cycles. Contrary to the hydro-morphodynamic model FLOW-3D, the hydro-morphodynamic model SedFoam allows to simulate the cycles of digging and refilling. Fig. 8 shows that the three-dimensional numerical hydro-morphodynamic model SedFoam can simulate cycles of digging and refilling starting from a flow rate  $Q$  higher than  $11.5 \text{ l/min}$ .

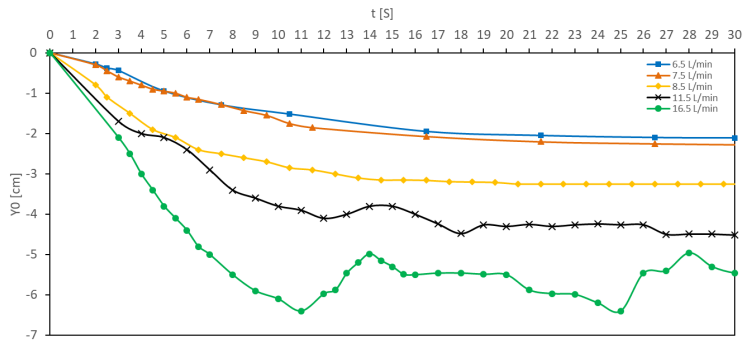


**Figure 8.** Time evolution of the maximum scour depth  $Y_0$  obtained by SedFOAM for different values of the flow rate  $Q = 6.5$  ( $\square$ ),  $7.5$  ( $\Delta$ ),  $8.5$  ( $\diamond$ ),  $11.5$  ( $\times$ ) and  $16.5$  ( $\circ$ )  $l/min$ .

## 5. Origin of observed mechanisms

### 5.1. Shape-shifting of the dune

This section is dedicated to understand the main cause of the shape-shifting of the dune. To explain the shape-shifting of the dune, the analysis of streamlines before, during and after this shape-shifting, obtained with both hydro-morphodynamic models, was performed for a flow rate of  $8.5 l/min$  (see Fig. 9). The shape-shifting can be considered as a hydro-morphodynamic phenomena that is explained by the interaction between the water flow and the dune. The streamlines allow to track the water flow path through the channel. This tracking of the water flow path showed a different behavior before, during and after the shape-shifting of the dune from a triangular shape to a trapezoidal shape.

In Fig. 9, it can be observed that SedFoam and FLOW-3D give generally the same behavior of streamlines. The two hydro-morphodynamic models present differences in the downstream and upstream recirculation zones. For the downstream recirculation zone, this can be explained by the fact that SedFoam does not solve a free surface flow unlike FLOW-3D. With SedFoam, the free surface is represented by a rigid patch on which a zero gradient boundary condition is applied. With FLOW-3D, the VOF method is used to simulate the free surface flow. The impact of the water jet on this surface is different between the two models. This produces a different effect on the recirculation zone located downstream of the dune. For the upstream recirculation zone, this can be explained by the fact that SedFoam can not use a mesh cell size lower than the mean grain size  $d_m$  of the sediment particles because of the dense granular flow rheology used by SedFOAM. It is impossible to refine the mesh in order to reduce the numerical instabilities observed. Fig. 10 presents the x-axis position of points where the jet impacts the dune start position and the free surface of water as a function of the time, obtained with SedFoam and FLOW-3D. It can be observed that the two hydro-morphodynamic models, SedFoam and FLOW-3D, give the same behavior of the jet at the upstream of the dune. The difference between SedFoam and FLOW-3D is about 1 to 3  $cm$ . The form, direction and characteristic of the jet are very similar for both models even though there are differences on the downstream and upstream recirculation zones obtained with SedFoam and FLOW-3D.

Fig. 9 ( $t = 7s$ ) shows that before the shape-shifting of the dune, the water jet follows the slope of the scour and the upstream side of the dune. The water jet propagates upward reaching the free surface and then follows the free surface in a quasi-straight flow vector. Fig. 9 ( $t = 12s$ ) shows that during the shape-shifting of the dune, the displacement of particles from the scour to the

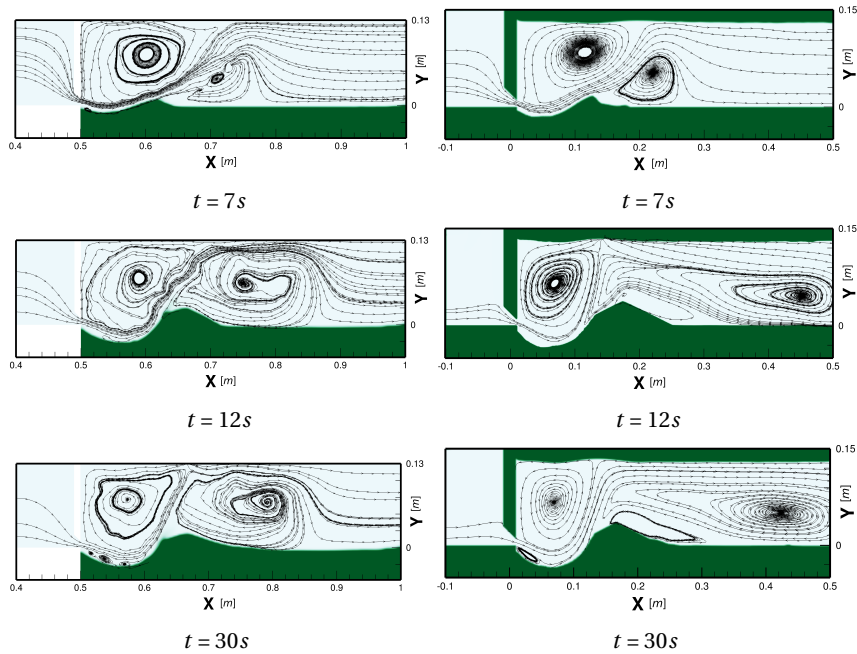


**Figure 9.** Streamlines of the flow before ( $t = 7s$ ), during ( $t = 12s$ ) and after ( $t = 30s$ ) the dune shape-shifting obtained by SedFoam (left) and FLOW-3D (right) for a flow rate  $Q = 8.5 \text{ l/min}$ .

upstream face of the dune by the jet causes an increase in the slope of this upstream face of the dune. The water jet following the slope of this upstream face of the dune becomes straighter. As the jet no longer impacts the free surface at the same place, the recirculation zone located downstream of the dune will be able to develop. As it develops, the recirculation zone breaks a part of the upstream face of the dune, producing two upstream faces called the first and second upstream faces. The trapezoidal shape then appears. Fig. 9 ( $t = 30s$ ) shows that after the shape-shifting of the dune, the scouring continues. Particles accumulate on the first upstream face of the dune. The water jet following this first upstream face of the dune straightens. This frees up the recirculation zone at the downstream side of the dune. The second upstream side of the dune is then no longer subject to this recirculation zone. The stationary regime then appears. In conclusion, this behavior of the hydrodynamics described earlier is the main origin of the shape shifting of the dune.

## 5.2. Digging-refilling cycles

To understand the origin of digging-refilling cycles, the spatial distribution of two components of the flow velocity in the  $x$  and  $y$  directions was presented in Fig. 11. The flow velocities presented are before ( $t = 9s$ ), during ( $t = 10s$ ) and after ( $t = 11s$ ) the first digging-refilling cycle obtained by SedFoam for a flow rate  $Q = 16.5 \text{ l/min}$ . In Fig. 11, it can be observed at  $t = 9s$  that the water jet is impacting the dune whether in the  $x$  or  $y$  direction, thus, providing positive sediment transport in the flow direction and providing a support to the dune mass. During the digging-refilling cycle (see Fig. 11 at  $t = 10s$ ), it can be observed that a recirculation zone inside the scour is formed. This recirculation zone pushed the water jet upward to the surface changing its direction. Now, the water jet does not impact the dune anymore and a negative flow at the left face of the dune

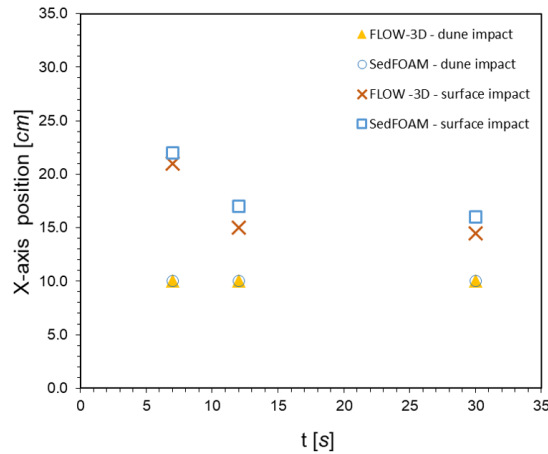


**Figure 10.** X-axis position of impact points of the jet on the dune start position (dune impact) and the free surface of water (surface impact) as a function of the time, obtained with SedFoam and FLOW-3D.

is presented indicating that the flow is not supporting the mass of the dune anymore. The face of the dune has a very steep slope, making it unstable. As there is no water flow supporting the dune mass anymore, this steep slope will cause an avalanche of the dune mass due to gravity. The scour will be filled. When the scour is refilled, the recirculation zone that made the jet goes upward dissipates instantly causing the water jet to take back its normal course and impacting the dune causing erosion in the scour and support to the dune (see Fig. 11 at  $t = 11$  s).

## 6. Analysis of observed mechanisms

### 6.1. Analysis of the turbulence

As it was complicated to measure the turbulence during the experimental procedure, one of the interests of numerical models is that we can have numerically the spatial distribution of the turbulence in the computational domain. Thus, the numerical results of both hydro-morphodynamic models can show and highlight the turbulence spatial and temporal evolution during the different phases of the erosion process. In Fig. 12, using the RNG  $k-\varepsilon$  model of FLOW-3D (see Eqs. (20) and (21)), the turbulence kinetic energy  $k_T$  (TKE) and the dissipation of the turbulent energy  $\varepsilon_T$  (DTKE) are represented for a flow rate  $Q = 8.5$  l/min at a time  $t = 30$  s in the middle of the channel and the left side near the wall during the stable dune phase considering that the jet is symmetric according to the mid plane. By means of these numerical results, we can analyze the hydrodynamics of the water jet from the turbulence. As seen in this figure, the zone with the highest values of the turbulent kinetic energy  $k_T$  (TKE) and the dissipation of the turbulent energy  $\varepsilon_T$  (DTKE) is directly after the sluice gate opening and inside the scour. The turbulence follows the water jet direction and decreases with the increasing distance from the sluice gate opening.

Additionally, it is observed that the turbulent kinetic energy  $k_T$  (TKE) and the dissipation of the turbulent kinetic energy  $\varepsilon_T$  (DTKE), near the wall, are lower than the mid plane. The numerical results emphasize the effect of the wall on the hydro-dynamics of the flow jet. For instance, the highest values of the turbulent kinetic energy  $k_T$  (TKE) and the dissipation of the turbulent



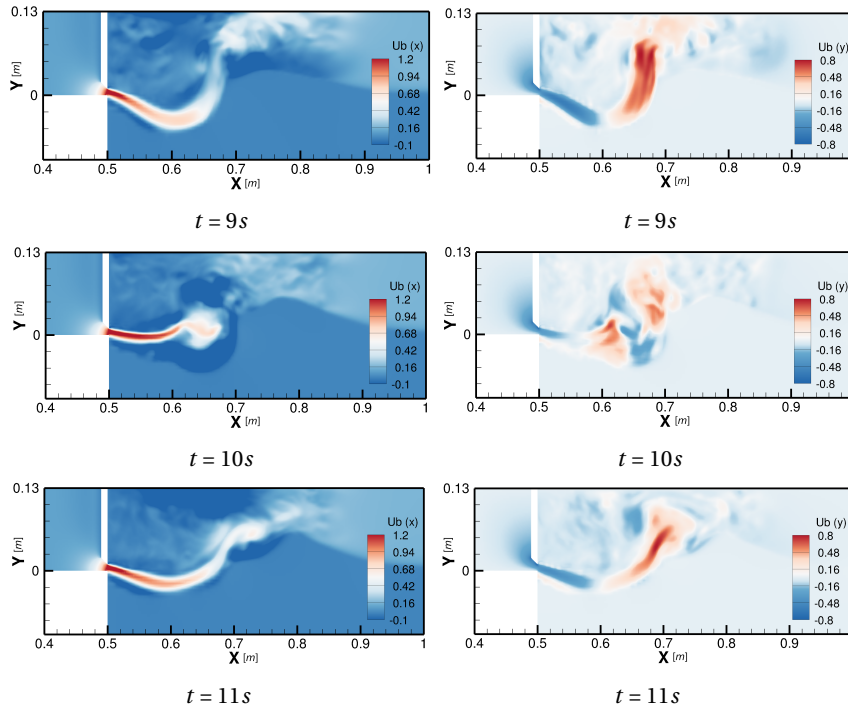


**Figure 11.** Components of the flow velocity in the  $x$  (left) and  $y$  (right) directions before ( $t = 9\text{ s}$ ), during ( $t = 10\text{ s}$ ) and after ( $t = 11\text{ s}$ ) the first digging-refilling cycle obtained by SedFoam for a flow rate  $Q = 16.5\text{ l/min}$ .

kinetic energy  $\varepsilon_T$  (DTKE) are respectively  $5 \times 10^{-5}\text{ m}^2 \cdot \text{s}^{-2}$  and  $2\text{ m}^2 \cdot \text{s}^{-3}$  in the mid plane while they are respectively  $2 \times 10^{-5}\text{ m}^2 \cdot \text{s}^{-2}$  and  $1\text{ m}^2 \cdot \text{s}^{-3}$  near the wall for the same region (see Fig. 12).

In Fig. 13, using the  $k-\omega$  model of SedFoam (see Eqs. (7) and (8)), the time evolution of the turbulent kinetic energy  $k$ , before ( $t = 7\text{ s}$ ), during ( $t = 17\text{ s}$  and  $18\text{ s}$ ) and after ( $t = 26\text{ s}$ ) the digging-refilling phase, is represented in the mid plane and near the left side wall. As seen in this figure, the highest value of the turbulent kinetic energy  $k$  is at the sluice gate opening ( $8 \times 10^{-5}\text{ m}^2 \cdot \text{s}^{-2}$ ) and inside the scour. It follows the water jet direction through the cavity with a value around  $5 \times 10^{-5}\text{ m}^2 \cdot \text{s}^{-2}$  (see Fig. 13  $t = 7\text{ s}$ ). When the water jet oscillates in the upward direction, it can notice that the turbulent kinetic energy  $k$  increases slightly ( $5.5 \times 10^{-5}\text{ m}^2 \cdot \text{s}^{-2}$ ) and follows the upward shifting of the water jet (see Fig. 13  $t = 17\text{ s}$ ). The turbulent kinetic energy  $k$  increases significantly ( $1 \times 10^{-4}\text{ m}^2 \cdot \text{s}^{-2}$ ) facing the unstable face of dune that collapses to fill the scour thus disturbing the flow jet (see Fig. 13  $t = 18\text{ s}$ ). Once the refilling phase is finished and a new digging phase is initiated, the turbulent kinetic energy  $k$  follows back the water jet direction all along the cavity and the dune (see Fig. 13  $t = 26\text{ s}$ ), taking its initial value of  $5 \times 10^{-5}\text{ m}^2 \cdot \text{s}^{-2}$  inside the scour. It is also observed that the values of the turbulence kinetic energy  $k$  near the wall are significantly lower than in the mid plane.  $Z$

## 6.2. Analysis of the shear stress and the sediment flux

Fig. 14 shows the shear induced pressure  $P^a$  representing the collision between the particles during the digging phase ( $t = 10\text{ s}$ ) and the refilling phase ( $t = 18\text{ s}$ ) obtained by SedFoam for a flow rate  $Q = 16.5\text{ l/min}$ . In Fig. 14, it is shown that during the digging phase ( $t = 10\text{ s}$ ), the highest



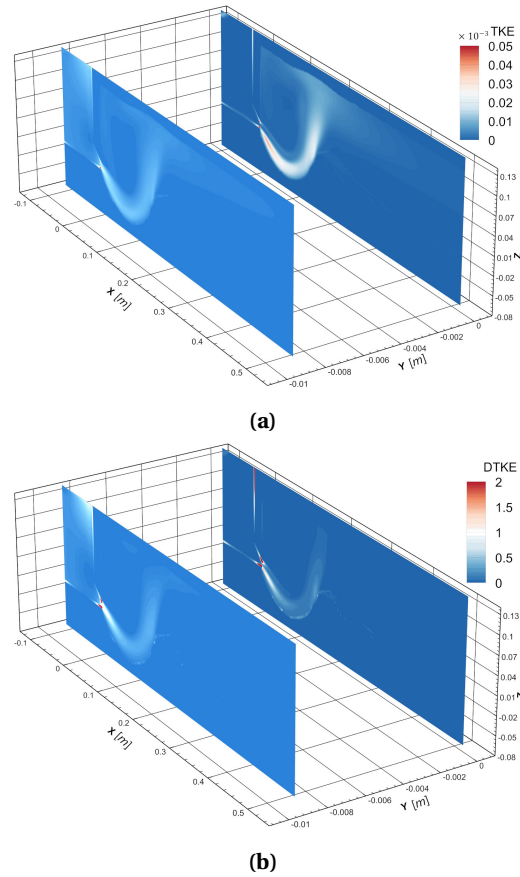


**Figure 12.** Spatial distribution of the turbulent kinetic energy  $k_T$  (TKE) and the dissipation of the turbulent kinetic energy  $\varepsilon_T$  (DTKE) along the flow jet obtained by FLOW-3D for a flow rate  $Q = 8.5 \text{ l/min}$  and a time  $t = 30 \text{ s}$ .

value of  $P^a$ , that is equal to  $3 Pa$ , is at the impinging zone at the downstream side of the scour and the upstream face of the dune, which indicates the collision of particles in this zone do to displacement and deposition while during the refilling phase ( $t = 18\text{s}$ ),  $P^a$  decreases significantly on the upper face of the dune and increases inside the scour, which indicates the presence of collision of particles inside the scour only due to the avalanche of particles.

Fig. 15 shows the component of the shear stress  $\tau_{xy}^a$  before ( $t = 10 \text{ s}$ ) and during ( $t = 18 \text{ s}$ ) the refilling phase obtained by SedFoam for a flow rate  $Q = 16.5 \text{ l/min}$ . The component of the shear stress  $\tau_{xy}^a$  follows the direction of the upstream slope of the dune in the particles phase. During the digging phase, it is the flow jet that induced high values of shear stress  $\tau_{xy}^a$  on the left side of the dune (see Fig. 15  $t = 10\text{s}$ ). The flow jet causes positive high shear stresses at the zones where the jet hits the dune and inside the scour hole in the direction of the flow,  $\tau_{xy}^a = 20 Pa$  in the mid plane and around  $10 Pa$  near the Walls, which causes erosion of the granular media. The negative shear stress zones, with  $\tau_{xy}^a = -20 Pa$  in the mid plane and  $-8 Pa$  near the walls, in this phase indicate small zones of recirculation whether inside the cavity or on the second face of the left side of the dune where recirculation causes this face to stabilize. This is considered a hydrodynamic phenomena. It's the fluid acting on the particle phase, as indicated in the equations (3) and (4) where the terms that include the shear stress and flow velocity are dominant.

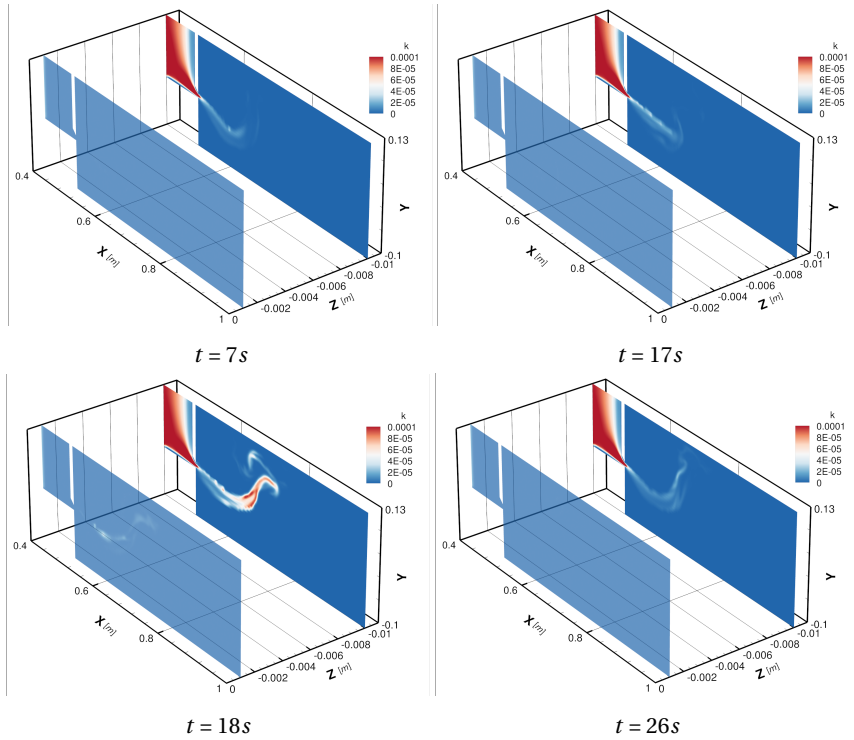


**Figure 13.** Spatial distribution of the turbulent kinetic energy  $k$  before ( $t = 7s$ ), during ( $t = 17$  and  $18s$ ) and after ( $t = 26s$ ) the digging-refilling phase of the scour obtained by SedFoam for a flow rate  $Q = 16.5 \text{ l/min}$ .

In contrast, during the refilling phase, it's not the flow jet that induces the shear induced pressure  $P^a$  and the component of the shear stress  $\tau_{xy}^a$ , since the jet was deviated upward (see Figs. 14 and 15  $t = 18s$ ). However, we still have high shear induced collision in the particles phase,  $P^a = 3 Pa$ , but just inside the scour whole while the value on the dune phase drops to around  $1 Pa$ , which is caused by the avalanche of the particles mass (see Fig. 14  $t = 18s$ ). On the other hand, the component of the shear stress  $\tau_{xy}^a$  on the left side of the dune changed from a positive value to a negative value equal to  $-20 Pa$ . This value is lower near the walls and take a value of around  $-7 Pa$  (see Fig. 15  $t = 18s$ ). Here, it is a geo-mechanical phenomenon where the driving motor is the gravity. As in the equations (3) and (4), the gravity term is the dominant since the flow of the jet doesn't interfere in this phase due to the upward shifting of the jet direction. During this phase, the component of the shear stress  $\tau_{xy}^a$  presents now negative values due to the direction of the avalanche of the particles mass that fills the cavity.

Fig. 16 presents the sediment flux before ( $t = 10 s$ ) and during ( $t = 18 s$ ) the refilling phase obtained by SedFoam for a flow rate  $Q = 16.5 \text{ l/min}$ . The sediment flux is given by the product between the particles concentration  $\alpha$  and the component of the particles velocity in the  $x$  direction,  $u_x^a$ . The sediment flux can be positive meaning it moves in the positive direction of the flow from the upstream to the downstream or negative meaning it moves in the opposed direction from the upstream to the downstream. The sediment flux showed that during normal situation of erosion a positive sediment flux is presented in the direction of the flow, moving from inside the scour all up the left side of the dune with a value that ranges from  $0.01$  and  $0.02 \text{ m/s}$ . It can be noted that the particles are moving along the scour and the dune and then follow the water jet in suspension to end up depositing on the dune.

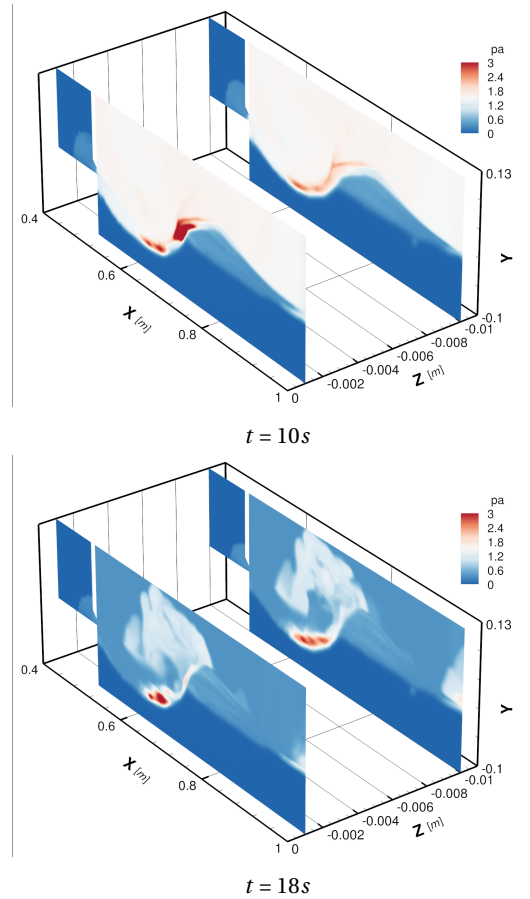


**Figure 14.** Spatial distribution of the shear induced pressure  $P^a$  during the digging phase ( $t = 10s$ ) and during the refilling phase ( $t = 18s$ ) obtained by SedFoam.

During the refilling phase, the sediments flux becomes negative indicating that the particles mass is moving in the opposed direction from the left side of the dune into the scour. Most importantly, this negative sediment flux is several times greater than the constant positive flux inside the scour during transport and erosion and it takes a value that ranges between  $-0.1$  and  $-0.06$   $m/s$  which means around 3 to 5 times greater than the digging phase. Thus, this high level of negative sediment flux indicates particles moving through the action of avalanche which means due to gravity and not by sediment transport by flow action on the bed.

## 7. Conclusions

The hydrodynamics of a water flow jet downstream of a submerged sluice gate and its impact on the granular bed made of cohesionless particles directly downstream of the gate based on an experimental study made by Martino et al. in 2019 [8] have been numerically studied using two different hydro-morphodynamic models. The first model, SedFoam, uses a coupled RANS modeling system for the coupling between the fluid phase and the particles phase and the second model, FLOW-3D, uses decoupling where the hydrodynamics is solved using RANS equations while the particles phase is modeled with a sediment transport scour model.

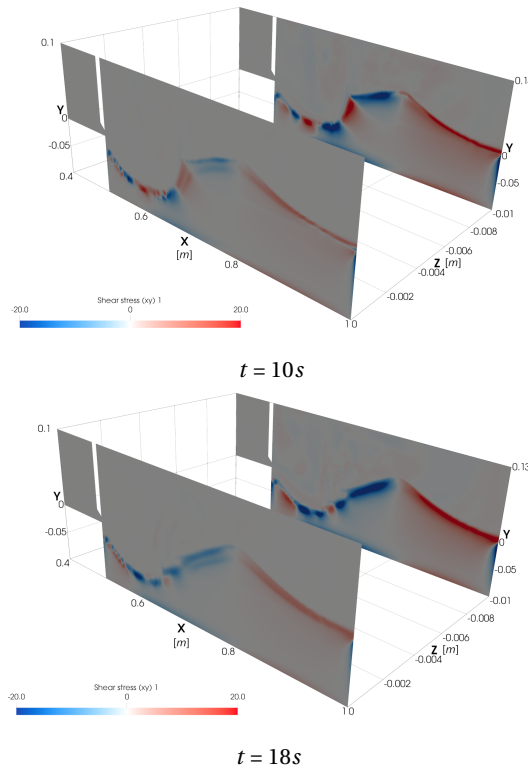


**Figure 15.** Spatial distribution of the component of the shear stress  $\tau_{xy}^a$  before ( $t = 10s$ ) and during ( $t = 18s$ ) the refilling phase obtained by SedFoam for a flow rate  $Q = 16.5 \text{ l/min}$ .

The two hydro-morphodynamic numerical models were first successfully calibrated to simulate the same flow profile and velocity decay of the experimental measurements and to simulate the behavior of the scouring and dune shape shifting phenomenon observed in the experimental measurements. Moreover, the three-dimensional numerical results served as an extended data base for the temporal and spatial evolution of streamlines, flow velocity, turbulence, shear induced pressure, shear stress, and sediment flux. These different physical quantities are complicated to have experimental measurements.

The three-dimensional numerical study highlighted the importance of the turbulent model on the stability of the numerical results in this some configurations and served as a detailed numerical data to explain the hydrodynamics of the water jet in contact with a confined granular bed and the morphological behaviour of the scour and dune observed in the experimental measurements.

This three-dimensional numerical study explained the evolution of the water jet hydrodynamics evolution in confined walls setup and its variation induced by the morphological changes. The analysis of numerical streamlines explained the origin of shape-shifting of the dune. The analysis of numerical flow velocity explained the origin of digging-refilling cycles. Furthermore, the three-dimensional numerical study helped highlight the differences between coupled and uncoupled hydro-morphodynamic numerical models. In this three-dimensional numerical study, the analysis of the turbulence, the shear induced pressure, the shear stress, and the sediment flux, allowed to describe the consequences of the avalanche of the particles mass.

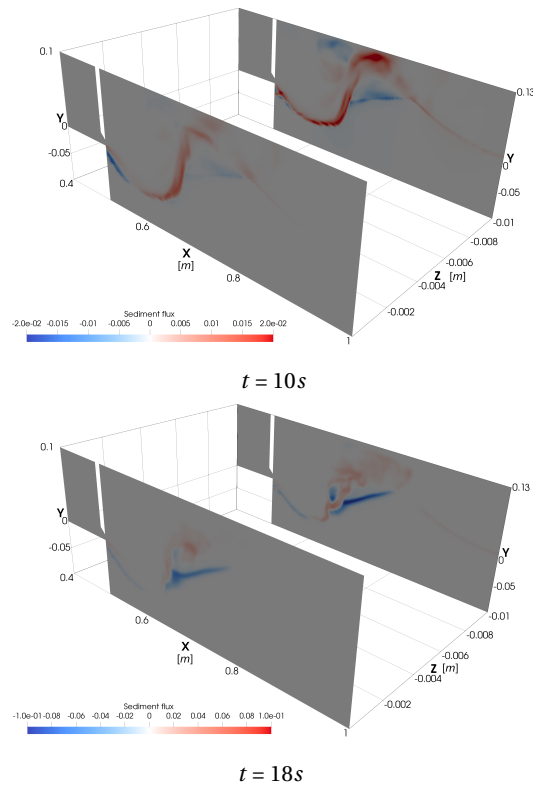


**Figure 16.** Spatial distribution of the sediment flux before ( $t = 10s$ ) and during ( $t = 18s$ ) the refilling phase obtained by SedFoam for a flow rate  $Q = 16.5 \text{ l/min}$ .

The use of three-dimensional hydro-morphodynamic models, as SedFoam and FLOW-3D, is nowadays possible to understand in depth the phenomena of scouring downstream of a sluice gate and formation of different shapes of dune in confined channels. The three-dimensional numerical study, presented in this work, allows to facilitate the choice of numerical methods for future numerical studies and to help mitigate certain numerical instabilities due to poor choice of numerical models whether its for the hydrodynamic, turbulence and transport models to be used.

### Declaration of competing interest

The authors declare that they have no known competing financial interests or personal relationships that could have appeared to influence the work reported in this paper.

### Acknowledgements

The authors very much appreciate the support of Julien Chauchat (associate professor) and Cyrille Bonamy (research engineer), whom represent the SedFOAM development team at LEGI labs and the university of Grenoble Alpes, for providing tutorials and guidance. The authors would also like to thank with gratitude, Marcelo F. Piva (professor) from Grupo de Medios Porosos at the University of Buenos Aires and Román G. Martino (researcher) from the Institute for Advanced Studies in Engineering and Technology, Universidad Nacional de Córdoba and

member of the National Scientific and Technical Research Council (CONICET) for providing experimental data.

## References

- [1] H. N. C. Breusers, A. J. Raudkivi, *Scouring*, Hydraulic Structures Design Manual Series, vol. 2, CRC Press, 2020.
- [2] P. Khwairakpam, A. Mazumdar, "Local Scour Around Hydraulic", *Int. J. Recent Trends Eng. Res.* **1** (2009), no. 6, p. 59-61.
- [3] C. Chevalier, D. P. v. Bang, E. Durand, I. Charles, G. Herrier, "Scour and erosion phenomena occurring in waterways - recent advances", in *Scour and Erosion: Proceedings of the 7th International Conference on Scour and Erosion*, CRC Press, 2014, p. 33-48.
- [4] M. S. Abdelmoaty, M. Zayed, "Using side flow jets as a scour countermeasure downstream of a sluice gate", *Beni-Suef Univ. J. Basic Appl. Sci.* **10** (2021), article no. 88.
- [5] B. W. Melville, A. J. Raudkivi, "Flow characteristics in local scour at bridge piers", *J. Hydraul. Res.* **15** (1997), no. 1, p. 373-380.
- [6] N. Rajaratnam, "Erosion by plane turbulent jet", *J. Hydraul. Res.* **19** (1981), no. 4, p. 339-358.
- [7] S.-Y. Lim, G. Yu, "Scouring Downstream of Sluice Gate", in *First International Conference on Scour of Foundations*, vol. USA. College Station, Texas, Texas Transportation Inst., Publications Dept., 2002, p. 395-409.
- [8] R. G. Martino, F. G. Ciani, A. Paterson, M. F. Piva, "Experimental study on the scour due to a water jet subjected to lateral confinement", *Eur. J. Mech. B Fluids* **75** (2019), p. 219-227.
- [9] S. Chatterjee, S. Ghosh, M. Chatterjee, "Local scour due to submerged horizontal jet", *J. Hydraul. Eng.* **120** (1994), no. 8, p. 973-992.
- [10] R. Balachandar, H. Reddy, "Sediment Transport Processes and their Modelling Applications" (A. J. Manning, ed.), InTech, 2013, p. 177-210.
- [11] C. Xie, S. Lim, "Effect of jet-flipping on scour development downstream of a sluice gate", 2012, 6th. International Conference on Scour and Erosion (ICSE 6), Paris, France.
- [12] A. Bey, M. Faruque, R. Balachandar, "Effects of varying submergence and channel width on local scour by plane turbulent wall jets", *J. Hydraul. Res.* **46** (2008), no. 6, p. 764-776.
- [13] J. Chauchat, Z. Cheng, T. Nagel, C. Bonamy, T. J. Hsu, "Sedfoam-2.0: a 3D two phase flow numerical model for sediment transport", *Geosci. Model Dev.* **10** (2017), p. 4367-4392.
- [14] Flow3d, "FLOW-3D Version 12.0", 2019, Santa Fe, NM: Flow Science, Inc., <https://www.flow3d.com>.
- [15] L. O. Amoudry, "Extension of  $k-\omega$  turbulence closure to twophase sediment transport modelling: Application to oscillatory sheet flows", *Adv. Water Resources* **72** (2014), p. 110-121.
- [16] GDR MiDi, "On dense granular flows", *Eur. Phys. J. E* **14** (2014), p. 341-365.
- [17] V. Yakhot, S. A. Orszag, "Renormalization group analysis of turbulence I. Basic theory", *J. Sci. Comput.* **1** (1986), p. 3-51.
- [18] V. Yakhot, L. M. Smith, "The renormalization group, the e-expansion and derivation of turbulence models", *J. Sci. Comput.* **7** (1992), p. 35-61.
- [19] P. Nielsen, *Coastal bottom boundary layers and sediment transport*, Advanced Series on Ocean Engineering, vol. 4, World Scientific, 1992.
- [20] E. Meyer-Peter, R. Müller, "Formulas for bed-load transport", in *Proceedings of the 2nd Meeting of the International Association for Hydraulic Structures Research*, Hydraulic Engineering Reports, IAHR, 1948, p. 39-64.
- [21] J. Chauchat, "A comprehensive two-phase flow model for unidirectional sheet-flows", *J. Hydraul. Res.* (2017), p. 1-14.
- [22] L. Schiller, A. Naumann, "Über die Grundlegenden Berechnungen bei der Schwerkraftaufbereitung", *Z. Vereines Deutscher Inge.* **77** (1933), p. 318-321.
- [23] K. Guizien, M. Dohmen-Janssen, G. Vittori, "1DV bottom boundary layer modeling under combined wave and current: Turbulent separation and phase lag effects", *J. Geophys. Res. Oceans* **108** (2003), article no. 3016.
- [24] H. Danon, M. Wolfshtein, G. Hetsroni, "Numerical calculations of two-phase turbulent round jet", *Int. J. Multiphase Flow* **3** (1977), p. 223-234.
- [25] C. P. Chen, P. E. Wood, "A turbulence closure model for dilute gas-particle flows", *Can. J. Chem. Eng.* **63** (1985), p. 349-360.
- [26] W. M. Kranenburg, T. J. Hsu, "Two-phase modeling of sheet-flow beneath waves and its dependence on grain size and streaming", *Adv. Water Resources* **72** (2014), p. 57-70.
- [27] Z. Cheng, T. J. Hsu, J. Calantoni, "SedFoam: A multidimensional Eulerian two-phase model for sediment transport and its application to momentary bed failure", *Coast. Eng.* **119** (2017), p. 32-50.
- [28] P. C. Johnson, R. Jackson, "Frictional-collisional constitutive relations for granular materials, with application to plane shearing", *J. Fluid Mech.* **176** (1987), p. 67-93.
- [29] P. Jop, Y. Forterre, O. Pouliquen, "A constitutive law for dense granular flows", *Nature* **441** (2006), p. 727-730.

- [30] E. Usta, "Numerical Investigation of Hydraulic Characteristics of Lalaei Dam Spillway and Comparison with Physical Model Study", PhD Thesis, Middle East Technical University, Ankara, Turkey, 2014.
- [31] C. W. Hirt, J. M. Sicilian, "A porosity technique for the definition of obstacles in rectangular cell meshes", in *Proceedings of the 4th International Conference on Numerical Ship Hydrodynamics, Washington DC, USA*, 1985.
- [32] R. Daneshfaraz, A. Ghaderi, A. Akhtari, S. D. Francesco, "On the Effect of Block Roughness in Ogee Spillways with Flip Buckets", *Fluids* **5** (2020), article no. 182.
- [33] H. Samma, A. Khosrojerd, M. Rostam-Abadi, M. Mehraein, Y. Cataño-Lopera, "Numerical simulation of scour and flow field over movable bed induced by a submerged wall jet", *J. Hydroinformatics* **22** (2020), no. 2, p. 385-401.
- [34] R. Soulsby, "Ch. 9: Bedload transport in Dynamics of Marine Sand", in *Dynamics of marine sands*, Thomas Telford Publishing, 1997.
- [35] L. C. V. Rijn, "Sediment Transport, Part I: Bed load transport", *J. Hydraul. Eng.* **110** (1984), no. 10, p. 1431-1456.
- [36] M. Ghasemi, S. Soltani-Gerdefaramarzi, "The Scour Bridge Simulation around a Cylindrical Pier Using Flow-3D", *J. Hydro-Environ Res.* **1** (2017), no. 2, p. 46-54.